



**Suppressing Defects Through Synergistic Effect of Lewis
Base and Lewis Acid for Highly Efficient and Stable
Perovskite Solar Cells**

Journal:	<i>Energy & Environmental Science</i>
Manuscript ID	EE-ART-08-2018-002252.R2
Article Type:	Paper
Date Submitted by the Author:	05-Oct-2018
Complete List of Authors:	Zhang, Fei; National Renewable Energy Laboratory, Chemistry and Nanoscience Center; Tianjin University, School of Chemical Engineering and Technology Bi, Dongqin; Ecole Polytechnique Federale de Lausanne Pellet, Norman; Ecole Polytechnique Federale de Lausanne Xiao, Chuanxiao; National Renewable Energy Laboratory, Li, Zhen; Northwestern Polytechnical University, State Key Laboratory of Solidification Processing, Center for Nano Energy Materials, School of Materials Science and Engineering Berry, Joseph; National Renewable Energy Laboratory (NREL), United States, National Center for Photovoltaics Zakeeruddin, Shaik Mohammed; Ecole polytechnique federale de Lausanne Institut des Sciences et Ingenierie Chimiques, ; Zhu, Kai; National Renewable Energy Laboratory, Chemical and Materials Science Center Grätzel, Michael; Swiss Federal Institute of Technology, Institut of Physical Chemistry

Broader context

Rapid development of perovskite solar cells (PSCs) during the past several years has made this photovoltaic (PV) technology a serious contender for potential large-scale deployment in the PV market. Achieving long term operational stability at high efficiency level for PSCs is the most challenging issue toward commercialization of this emerging PV technology. Here, we demonstrate PSCs with simultaneously improved device performance and stability by combining Lewis base BrPh-ThR and Lewis acid bis-PCBM during device fabrication for the first time. Using both Lewis base and acid can enhance resistance to moisture incursion, passivate defects in the absorber layer, and suppress pinholes generated in the hole-transporting layer. The combination of Lewis base BrPh-ThR and Lewis acid bis-PCBM positively enhances the crystallization, mobility, and conductivity of perovskites, leading to improved device efficiency from 19.3% to 21.7%. The unsealed devices remained at 93% of the initial efficiency value in ambient air (10%–20% relative humidity) after 3,600 h at 20–25 °C and dropped by 10% after 1,500 h under continuous operation at 1-sun illumination and 55°C in nitrogen with maximum power-point tracking. This promising approach provides a simple route for fabricating highly efficient and stable PSCs.



Suppressing Defects Through Synergistic Effect of Lewis Base and Lewis Acid for Highly Efficient and Stable Perovskite Solar Cells

Fei Zhang,^{1,2} Dongqin Bi,³ Norman Pellet,² Chuanxiao Xiao,¹ Zhen Li,¹ Joseph J. Berry,¹ Shaik Mohammed Zakeeruddin,² Kai Zhu,^{1,*} Michael Grätzel^{2*}

Received 00th January 20xx,
Accepted 00th January 20xx

DOI: 10.1039/x0xx00000x

www.rsc.org/

Achieving long-term operational stability at high efficiency level for perovskite solar cells is the most challenging issue toward commercialization of this emerging photovoltaic technology. Here, we investigated the cooperation of Lewis base and Lewis acid by combining the commercial bis-PCBM mixed isomers as Lewis acid in the antisolvent and N-(4-bromophenyl)thiourea (BrPh-ThR) as Lewis base in the perovskite solution precursor. The combination of Lewis base and Lewis acid synergistically passivates Pb²⁺ and PbX³⁻ antisite defects, enlarges perovskite grain size, and improves charge-carrier separation and transport, leading to improved device efficiency from 19.3% to 21.7%. In addition, this Lewis base and acid combination also suppresses moisture incursion and passivates pinholes generated in the hole-transporting layer. The unsealed devices remained at 93% of the initial efficiency value in ambient air (10%–20% relative humidity) after 3,600 h at 20–25 °C and dropped by 10% after 1,500 h under continuous operation at 1-sun illumination and 55°C in nitrogen with maximum power-point tracking.

Introduction

Perovskite solar cells (PSCs) have attracted significant attention due to their high power conversion efficiency (PCE) and potential low cost. In only eight years, their PCEs have increased dramatically from 3.8% to more than 22%.^{1–4} To date, many fabrication methods have been proposed and demonstrated to produce high-quality perovskite films.^{5–10} Among them, the antisolvent-assisted one-step method is a well-proven effective strategy for obtaining perovskite films with good uniformity and suitable grain sizes.^{5,10}

In high-quality perovskite polycrystalline films, the bulk defect densities are often lower than the surface trap densities, contributing to the high PCE of PSCs.¹¹ Grain boundaries (GBs) as well as the surfaces in the perovskite thin films can significantly affect charge transport, recombination kinetics, device performance, and stability.¹² Owing to the ionic character of solution-processed perovskite semiconductors, the inherent

ionic defects in the perovskite can also bring some undesired issues, such as hysteresis behavior and device instability.^{13,14} These and other results indicate that defect-induced electronic trap states at the perovskite surface and GBs should be minimized for optimal device performance. Post-passivation treatment has been demonstrated to be an effective strategy to reduce the defect density in the perovskite films via bonding with uncoordinated halide or metal ions from perovskite crystals.^{15,16} It was demonstrated that the treatment of perovskite crystal surfaces with Lewis base molecules (such as thiophene, pyridine, thiourea, TDZDT, IT-M, 2-pyridylthiourea, DR3T etc) could efficiently passivate the under-coordinated Pb atoms and thus improve performance and stability.^{15,17–27} Phenyl-C61-butyric acid methyl ester (PCBM),^{28–30} potassium iodide (KI),^{31, 32} and zinc chloride (ZnCl)³³ as Lewis acid were also applied in the perovskite-solution precursor to improve film formation and increase environmental stability. Realizing stability at these efficiencies is critical to advancing PSCs, and the degradation in perovskite-based solar cells can stem from a myriad of sources within the device.³⁴ The deleterious impact of the intrusion of water/oxygen molecules into the perovskite active-layer are well documented but can be relieved via engineering of the interfaces within the device stack.³⁵ Moreover, recent studies show that defects, likely prevalent at GBs, play

¹ National Renewable Energy Laboratory, Golden, Colorado 80401, USA (email: kai.zhu@nrel.gov)

² Laboratory of Photonics and Interfaces, Institute of Chemical Sciences and Engineering, École Polytechnique Fédérale de Lausanne (EPFL), Station 6 CH-1015, Lausanne, Switzerland (email: michael.gratzel@epfl.ch)

³ School Of Materials Science and Technology, Sun Yat-sen University

Electronic Supplementary Information (ESI) available: See DOI: 10.1039/x0xx00000x

an important role in triggering the moisture-induced degradation process.

In this paper, we applied the commercial bis-PCBM mixed isomers as Lewis acid in the antisolvent and N-(4-bromophenyl)thiourea (BrPh-ThR) as Lewis base in the perovskite-solution precursor to investigate the cooperation of Lewis base and Lewis acid. Lewis acids can accept an electron from the negative-charged Pb-I antisite defects (PbI_3^-) or under-coordinated halide ions, and thus, passivate the halide-induced deep traps.³⁶⁻³⁸ Lewis bases usually function as electron donors, which can bind to the positively charged under-coordinated Pb^{2+} ions.¹⁷⁻²² However, most of these passivation molecules should only passivate one type of defect. Our results show that the synergistic combination of Lewis base and Lewis acid can passivate both defects, enlarge perovskite grain size, and improve charge-carrier separation and transport. Thus, compared with 19.3% for control, a PCE of 20.4% is obtained for only using BrPh-ThR in the precursor, 20.5% for only using bis-PCBM in the antisolvent, and a PCE of 21.7% when combining the bis-PCBM-laced antisolvent along with BrPh-ThR in the precursor. Importantly, this PCE remained at 93% and 90% of the initial value, respectively, after 3,600 h in ambient air (10%–20% relative humidity) at 20–25 °C and after 1,500 h under continuous full-sun illumination at maximum power-point tracking.

Result and discussion

A schematic illustration of the Lewis acid- and Lewis base-assisted growth process for the perovskite layer is shown in **Figure 1**. The mixed-cation perovskite $[(\text{FAI})_{0.81}(\text{PbI}_2)_{0.85}(\text{MABr})_{0.15}(\text{PbBr}_2)_{0.15}]$ precursor is prepared from a solution of formamidinium iodide (FAI), PbI_2 , methylammonium bromide (MABr), and PbBr_2 in a mixed solvent of dimethyl formamide (DMF) and dimethyl sulfoxide (DMSO) with 1.35 M Pb^{2+} (PbI_2 and PbBr_2) and certain amount of BrPh-ThR. This precursor is then spin-coated on mesoporous TiO_2 . During the last 15 s of a second spin-coating step, 110 μL of bis-PCBM containing chlorobenzene (CB) is dropped onto the above film to promote the formation of an intermediate phase and the cooperation of Lewis base BrPh-ThR. The BrPh-ThR as an S-donor has a strong ability to coordinate with PbI_2 to gain the flexibility of tuning the coordination strength which is beneficial for the perovskite formation process and passivating the Pb^{2+} defects as a bifunctional Lewis base. The bis-PCBM is expected to improve the grain size and facilitate perovskite growth in its preferred direction. The intermolecular force of BrPh-ThR with benzene ring may cause the molecular polymerization to destroy the ordered structure and affect the electron transport. The bis-PCBM can also passivate the key PbX_3^- antisite defects and lead to better dispersion of BrPh-ThR. As a result, the

interaction of the two molecules can work synergistically.

To examine this hypothesis, we performed liquid-state ^1H nuclear magnetic resonance (^1H NMR) spectroscopy and the results are shown in **Figures S1 and S2**. When adding some PbI_2 in the solution, the signals of -NH- and - NH_2 in the BrPh-ThR and - CH_3 in bis-PCBM were all shifted, indicating the formation of $-\text{C}=\text{S}\cdot\text{Pb}$ and $-\text{C}=\text{O}-\text{R}-\text{C}=\text{O}\cdot\text{Pb}$, respectively. The presence of $[(\text{FAI})_{0.81}(\text{PbI}_2)_{0.85}(\text{MABr})_{0.15}(\text{PbBr}_2)_{0.15}]$ induces a stronger chemical shift than that in the PbI_2 solution, indicating the possible formation of $\text{MA}(\text{FA})\text{I}(\text{Br})\cdot\text{Br}-\text{C}=\text{S}\cdot\text{Pb}$ and $\text{MA}(\text{FA})\text{I}(\text{Br})\cdot-\text{C}=\text{O}-\text{R}-\text{C}=\text{O}\cdot\text{Pb}$, respectively. When we added BrPh-ThR and bis-PCBM in the perovskite solution at the same time, the chemical shift was larger than that using either BrPh-ThR or bis-PCBM, indicating the synergistic effect from the cooperation of these two compounds.

To get insight into the surface-defect passivation effect of BrPh-ThR and bis-PCBM for perovskite films, we performed photoluminescence (PL) and time-resolved PL (TRPL) decay measurements for the corresponding samples on a glass substrate. When compared with the pristine perovskite film, the normalized steady-state PL spectra, shown in **Figure 2a**, indicates blue shifting of 4 nm, 5 nm, and 7 nm, respectively, for BrPh-ThR-containing (referred to as **Type A**), bis-PCBM-containing (referred to as **Type B**), and BrPh-ThR along with bis-PCBM-containing (referred to as **Type C**) perovskite layers as shown in **Figure 2a**. Such blue shifting and line narrowing is attributed to a decrease of spontaneous non-radiative recombination from trap states, which could account for the increased open-circuit voltage (V_{oc}) and fill factor (FF).³⁹ TRPL decay data are presented in **Figure 2b** and fitted to the **equation S3** derived in the supporting information.⁴⁰ This equation was reduced to an exponential rate law at longer times. Linear fits of the curves in the time domain are excellent, as shown in **Figure S3**, and yield the lifetimes for nonradiative carrier recombination listed in **Table S1**. The lifetimes follow the order: Type C film > Type B film > Type A film > pristine control perovskite film. This further confirms the synergistic effect of using both Lewis base (BrPh-ThR) and Lewis acid (bis-PCBM) on passivating defects in perovskite films, which again is consistent with the higher V_{oc} and FF of the corresponding PSC.⁴¹

To assess the defect density and charge transport, we conducted space-charge-limited current (SCLC) measurements of the corresponding perovskite films; the current density-voltage (J–V) characteristics of the different devices are shown in **Figure S4** and corresponding data are summarized in **Figure 2c**. Typical three regions I–V curves were observed in both devices in a log–log representation. In the low-bias region, the current density is proportional to voltage, which reflects an ohmic contact with the electrode.

With increasing bias, the current density increased abruptly, corresponding to a trap-filled limit (TFL) current.⁴² We calculated the trap-state density (N_t) using the TFL voltage equation $N_t = 2\epsilon\epsilon_0 V_{\text{TFL}}/qd^2$, where ϵ_0 is the dielectric constant of vacuum permittivity, ϵ is the relative dielectric constant of perovskite, q is the elementary charge, d is the thickness of the perovskite film, and V_{TFL} is determined from the J - V curve.⁴³ The presumptions of this analysis may be questioned in the context of the halide perovskite materials; however, it provides a relative measure of the trap densities and we can estimate the

trap densities for corresponding perovskite films. The trap density of **Type C** perovskite film is substantially lower than that of the other three films, which is consistent with the PL/TRPL results as well as the higher V_{oc} and FF in PSCs. We also calculated the mobility of the different perovskite films using the equation $J = 9\epsilon\epsilon_0\mu V^2/8d^2$. The mobility values were estimated to be 9.26, 13.71, 16.52, and 20.91 $\text{cm}^2 \text{V}^{-1} \text{S}^{-1}$, respectively, for pristine, **Type A**, **Type B**, and **Type C** perovskite films. The improved mobility and lifetime are consistent with the higher short-circuit voltage (J_{sc}) and FF of the corresponding PSCs.⁴⁴

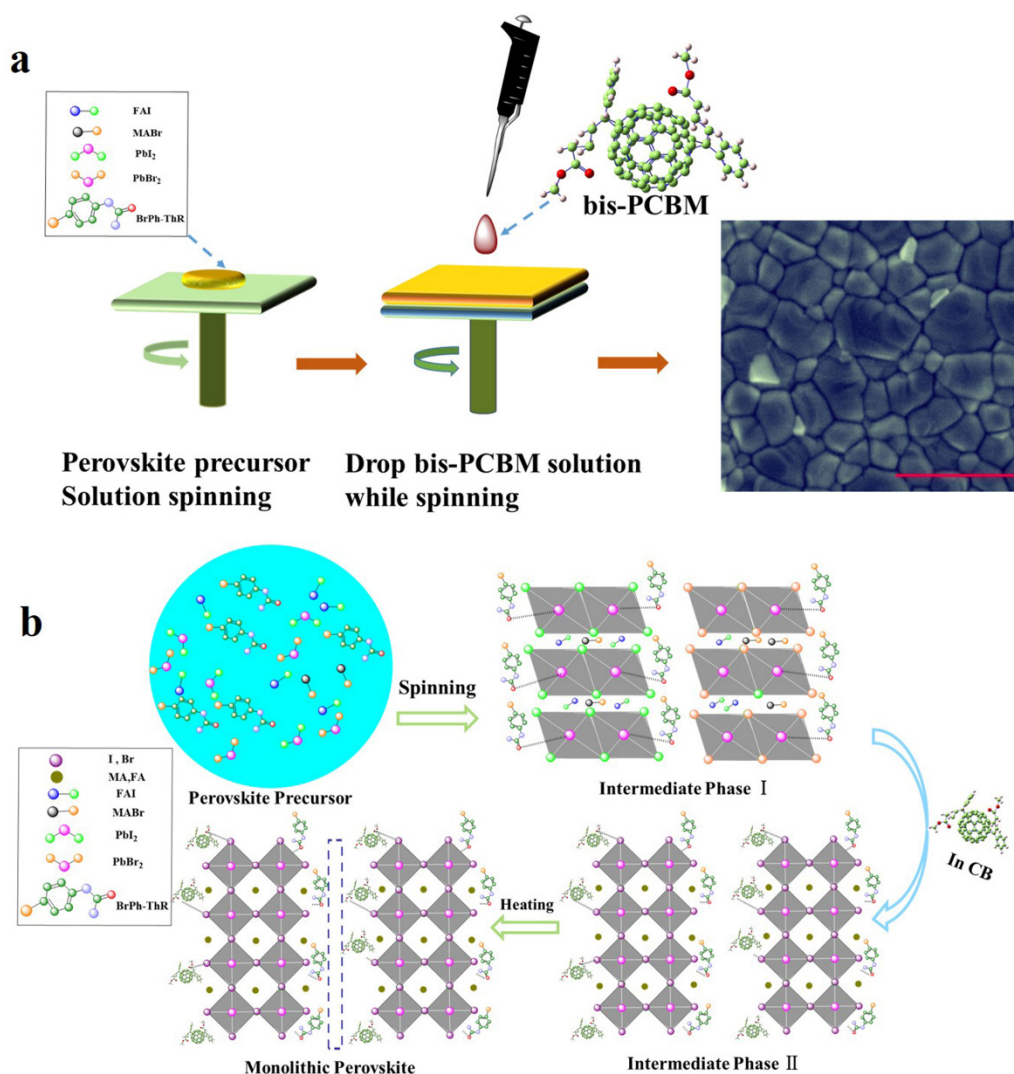


Figure 1 (a) Schematic diagram of antisolvent process; (b) Schematic reaction process of perovskite growth resulting from combination of the Lewis base BrPh-ThR in the perovskite-solution precursor and the Lewis acid bis-PCBM in the antisolvent process.

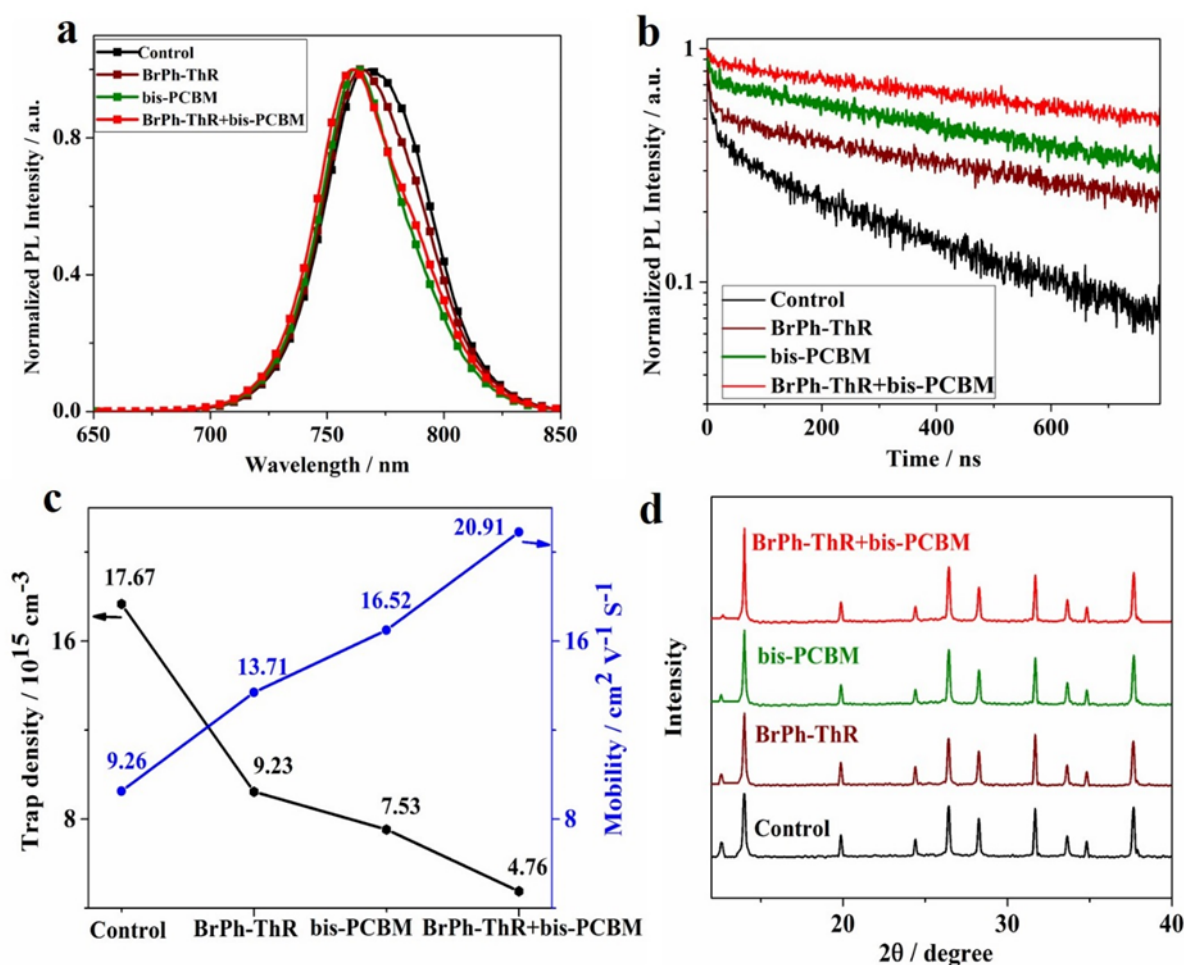


Figure 2 a) PL spectra; b) TRPL spectra of corresponding films on glass substrate; (c) trap density and mobility data of corresponding films obtained from SCLC method; (d) XRD patterns of corresponding films on meso-TiO₂/ compact TiO₂ / FTO substrate.

It is generally established that localized defects in the perovskite GBs and grain interiors (GIs) may serve as recombination centers, which are detrimental to PSC performance. Moreover, these localized defects may result in inefficient photo carrier separation and transport, leading to poor conducting properties of perovskite films.^{22,45} We carried out conductive atomic force microscopy (c-AFM) to investigate conducting properties of corresponding perovskite films. As shown in **Figure S5c-f**, the control sample showed comparatively low current signal, which indicates poor electrical conductivity of the perovskite films. In contrast, the perovskite films with BrPh-ThR and bis-PCBM present a significantly increased current signal at both the GBs and GIs, which suggests that surface trap states can be efficiently passivated with BrPh-ThR and bis-PCBM; this correlates well with decreased trap density

(SCLC) and improved carrier lifetime (TRPL). It is worth noting that the GBs show brighter contrast than GIs, revealing relatively higher current flow associated with more efficient charge transfer, which is in good agreement with the previous report.⁴⁶

The X-ray diffraction (XRD) measurements were performed to study the crystalline structure of perovskite films on m-TiO₂/c-TiO₂/FTO substrates (**Figure 2d**). The XRD patterns depict a set of characteristic peaks, which indicate tetragonal perovskite structure. XRD spectra exhibit similar, strong, and sharp perovskite characteristic peaks. The intensity of **Type C** perovskite film at (110) peak becomes stronger and the full width at half maximum (FWHM) decreased (**Figure S6a,b**) when compared with the pristine/**Type B**/**Type C** perovskite films; it shows that bis-PCBM and BrPh-ThR can improve the crystallization of

perovskite and/or more-preferred (110) orientation. We attribute the improved crystallization process to the templating effect of bis-PCBM and BrPh-ThR on the crystal growth. We ascribe the high-quality crystallization as one of the main factors for improved device performance.⁴⁷

Scanning electron microscopy (SEM) images of the corresponding perovskite films deposited on m-TiO₂/c-TiO₂/FTO substrate are presented in **Figure 3**. As illustrated from the top-view SEM, the change in morphology is consistent with an increase in grain size of the perovskite film with the use of either BrPh-ThR or bis-PCBM, and it directs most GBs to assume a perpendicular orientation to the substrate. After the use of both, the grain size becomes larger and thus it reduces the GB density. Hence, BrPh-ThR along with bis-PCBM appears to improve the grain size and facilitate perovskite growth with preferred direction. The morphology of the perovskite thin films with and without BrPh-ThR and bis-PCBM were further studied by AFM, as shown in **Figure S5a, b**. It can be found that with BrPh-ThR and bis-PCBM, the root-mean-square (rms) roughness of the perovskite film became smaller than that of the control films. The result shows that with the cooperation of BrPh-ThR and bis-PCBM, the perovskite thin film can be smoother and more uniform, which are beneficial for effective charge transport and higher photovoltaic performance.⁴⁸ **Figure S6c** presents the absorption spectra of the corresponding films. Compared with the pristine control perovskite film, obvious absorption enhancement is observed in almost the entire visible-light region for perovskite films using BrPh-ThR and/or bis-PCBM; this enhancement likely originates from the contribution of their impact on larger grain size and more uniform crystal formation of perovskite. These results could contribute to the much enhanced *J*_{sc} in the corresponding PSCs.

Figure 4a shows contact-angle measurements of a deionized water droplet with the corresponding perovskite film. The derived contact angles are 57.6°, 68.1°, 69.2°, and 77.8°, respectively, for the pristine, **Type A**, **Type B**, and **Type C** films. This trend reflects a strong increase in hydrophobicity of the perovskite upon incorporation of the BrPh-ThR along with bis-PCBM, resulting in its greatly enhanced stability against degradation in humid air. We exposed unsealed films of pristine, **Type A**, **Type B**, and **Type C** perovskite thin films to ambient environment of 45% relative humidity, and periodically recorded their XRD patterns as shown in **Figure 4b**. The decomposition of perovskite in moist air is known to lead to the formation of a PbI₂ phase. The ratio of PbI₂ ($2\theta = 12.5^\circ$) to perovskite ($2\theta = 13.8^\circ$) of pristine control perovskite increases faster than that of **Type A**, **Type B**, and **Type C** perovskite film after 30 days. The **Type C** perovskite film turned out to be the most stable one in this test environment, indicating that stability is improved after the Lewis acid and Lewis base cooperation. The enhanced stability of the **Type C** perovskite film can also be seen from **Figure 4c**, which shows that the color of the **Type C** perovskite film remains persistent; whereas, those of the **Type A** and **Type B** perovskite films change slightly and pristine control perovskite film almost turned to yellow.

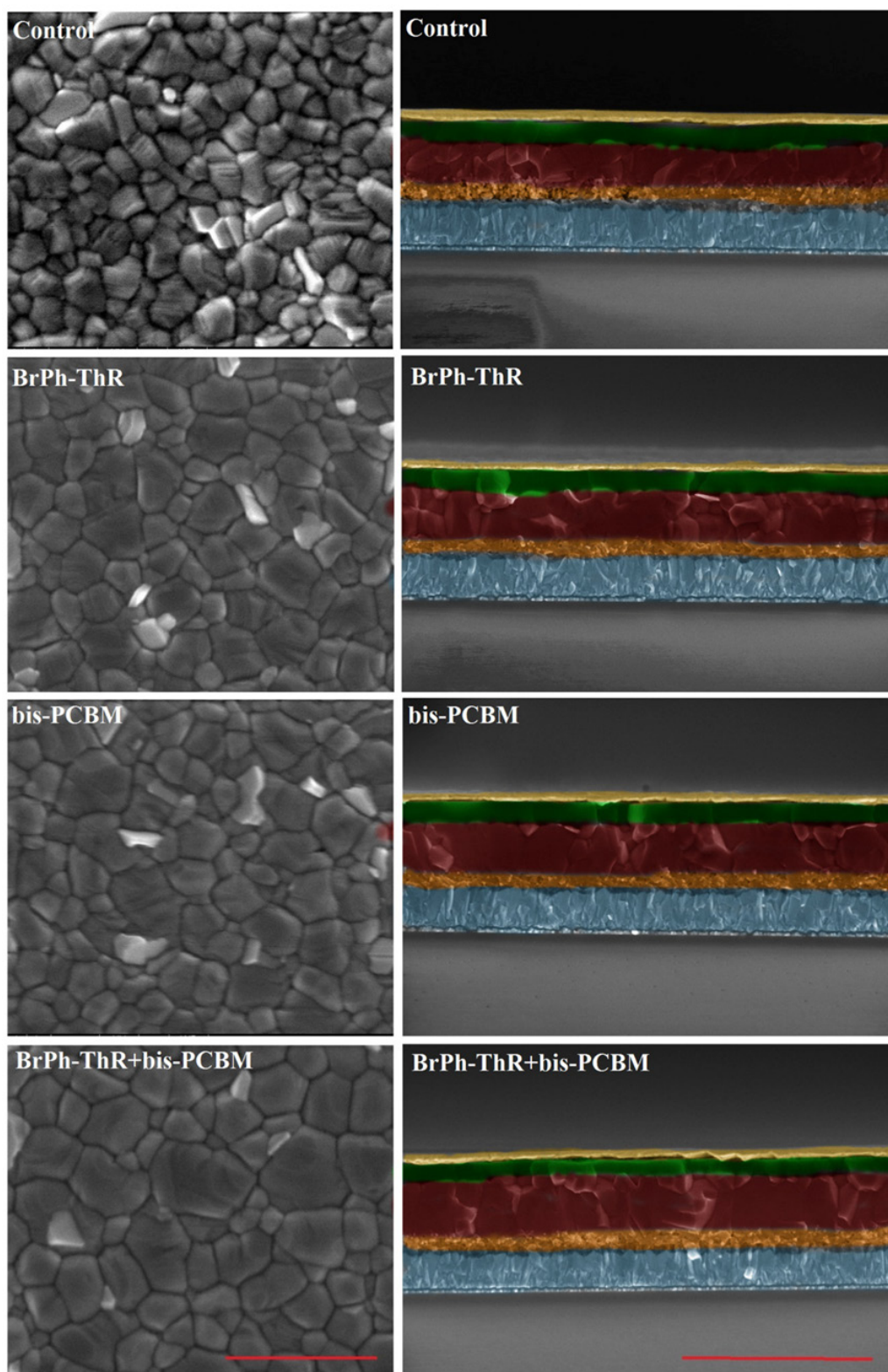


Figure 3 Scanning electron microscopy images. Top (left, the scale is 1 μm) SEM of corresponding perovskite films and cross-sectional (right, the scale is 2 μm) SEM of corresponding perovskite devices. 1, Control; 2, BrPh-ThR; 3, bis-PCBM; 4, BrPh-ThR + bis-PCBM.

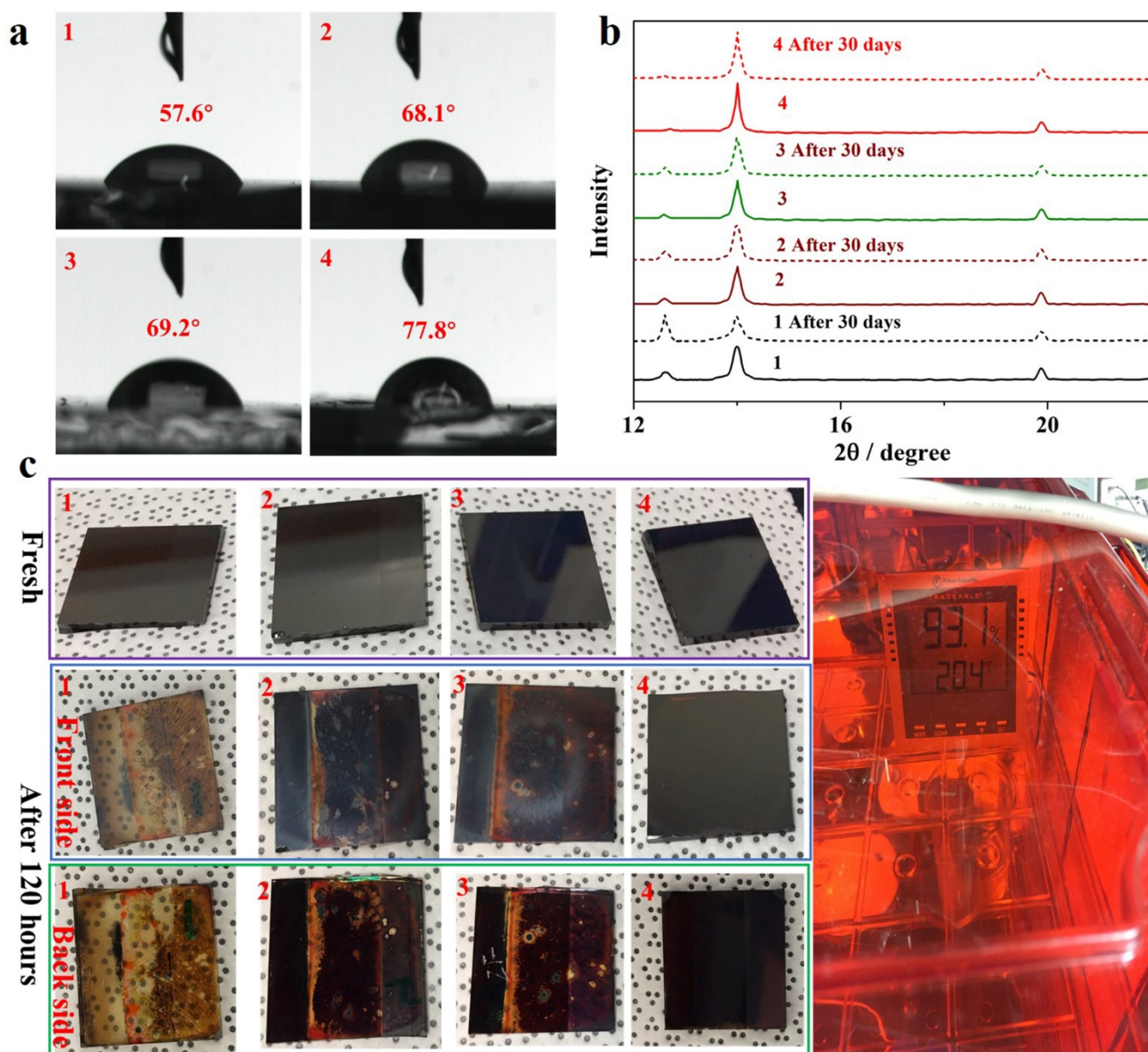


Figure 4 a) The contact angles between corresponding perovskite films and water; b) XRD patterns of corresponding films on meso-TiO₂/ compact TiO₂/ FTO substrate, which were exposed to ambient 45% relative humidity before and after 30 days; c) Photos of the corresponding films before and after aging to ambient 93% relative humidity for 120 hours; the first line is fresh films and the second and third line are frontside and backside of aging films, respectively. 1, Control; 2, BrPh-ThR; 3, bis-PCBM; 4, BrPh-ThR + bis-PCBM.

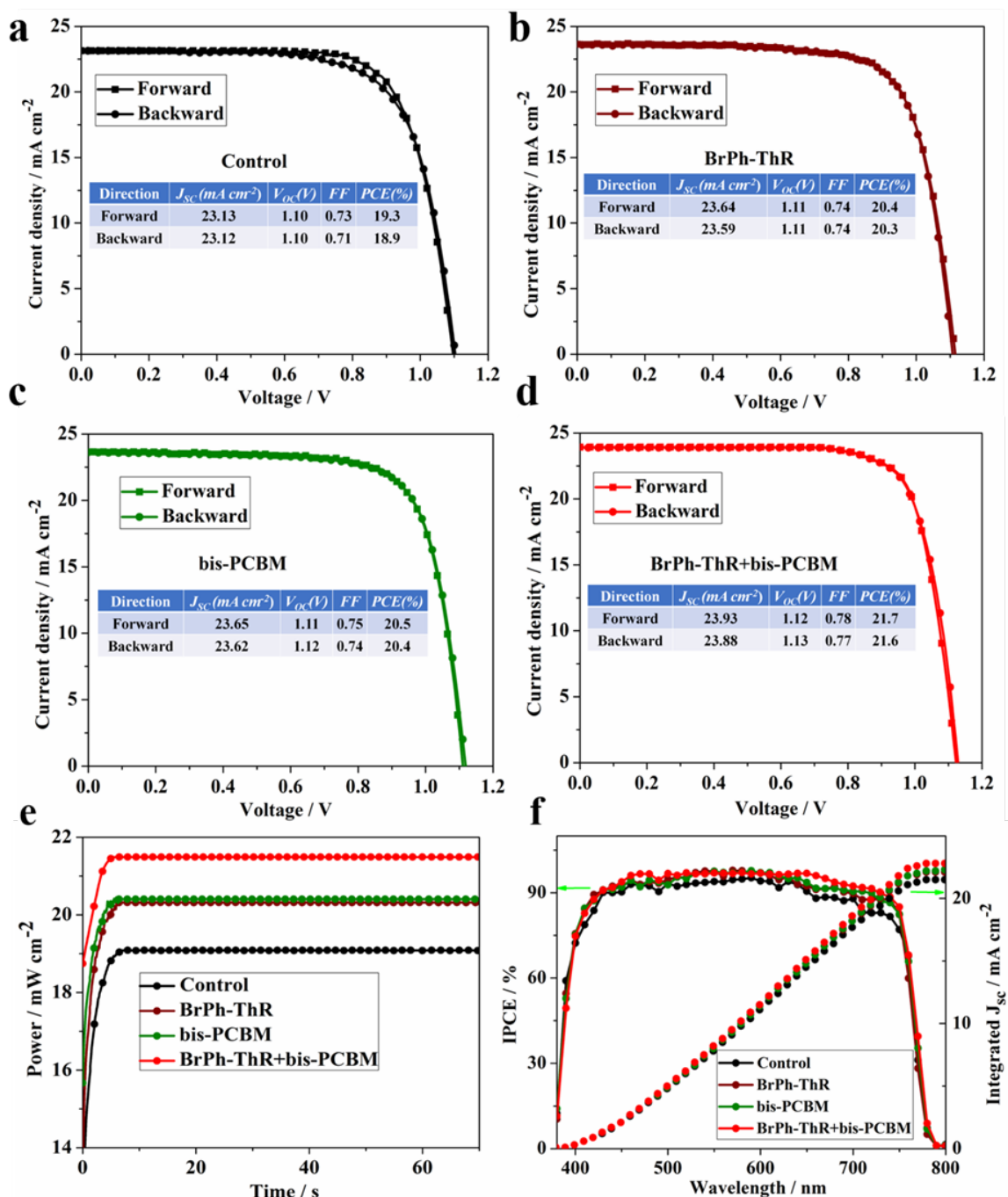


Figure 5 Current-voltage hysteresis curves of perovskite solar cells comprising champion devices measured starting with backward scan and continuing with forward scan with a bias step of 5 mV. a) control; b) BrPh-ThR; c) bis-PCBM; d) BrPh-ThR + bis-PCBM; e) the stabilized power output of the corresponding devices; f) IPCE spectra and integrated current curves of the corresponding devices.

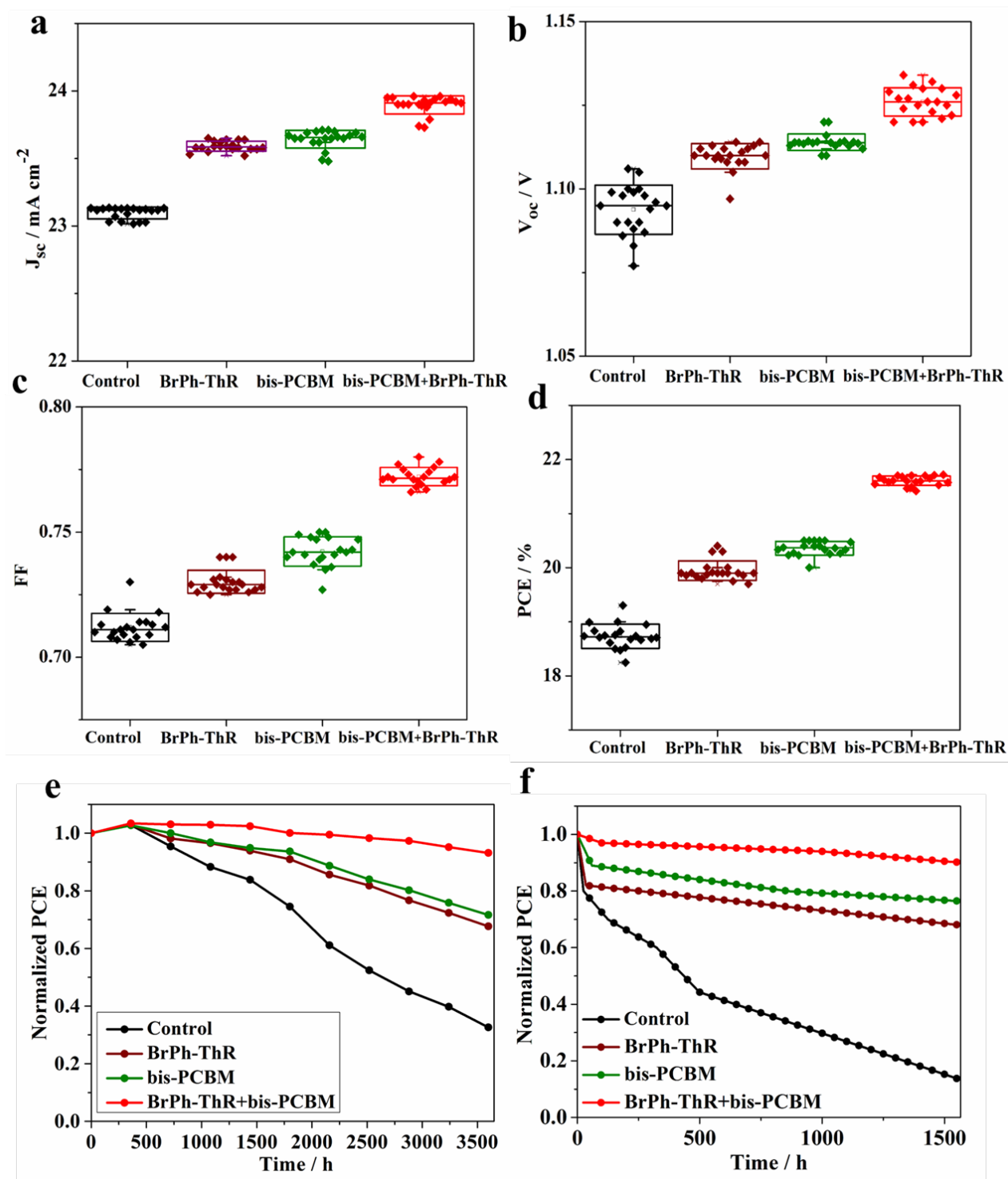


Figure 6 Photovoltaic metrics of devices based on corresponding perovskite layers. a) J_{sc} ; b) V_{oc} ; c) FF; d) PCE; e) the stability of corresponding perovskite solar cells in ambient environment of 10%–20% relative humidity dark storage without any encapsulation at 20–25 °C; f) the stability of corresponding perovskite solar cells under continuous full-sun illumination and maximum power-point tracking in a nitrogen atmosphere at 55 °C.

The cell architecture in this study adopted the traditional mesoporous structure with a full device stack Au / spiro-OMeTAD / perovskite / mesoporous TiO₂ / compact TiO₂ / FTO. The typical *J*-*V* curves of pristine, **Type A**, **Type B**, and **Type C** perovskite-based PSCs under AM 1.5 G illumination with the light intensity of 100 mW cm⁻² are shown in **Figure 5a-d**, and corresponding data were summarized in **Table S2**. The control device delivers a champion PCE of 19.3%, with *V*_{oc} of 1.10 V, *J*_{sc} of 23.13 mA cm⁻², and *FF* of 0.73, which is consistent with a previous report.⁴⁹ In contrast, **Type A**, **Type B**, and **Type C** perovskite-based devices displayed better performance with PCEs of 20.4%, 20.5%, and 21.7%, respectively. As previously reported,^{19,28} Lewis acid bis-PCBM or Lewis base thiourea plays a critical role in improving the quality of the active layer with larger grains and fewer grain boundaries, which result in obviously enhanced *J*_{sc} and *FF*. This study shows that combination of Lewis base and Lewis acid substantially enhances cell performance. We ascribed the improved *J*_{sc} and *FF* with Type C perovskite to mainly the higher conductivity (**Figure S5**), higher mobility (**Figure 2c**, **Table S3**), lower trap density, and larger grains and fewer grain boundaries. The hysteresis loss calculated from the equation

$$\text{Hysteresis loss \%} = \frac{P_{\text{forward}} - P_{\text{backward}}}{P_{\text{forward}}}$$

of devices based on pristine, **Type A**, **Type B**, and **Type C** perovskite films are 2.08%, 0.49%, 0.48%, and 0.46%, respectively. The origination of hysteresis in PSCs is reported to be due to the trap state of charge carriers, ion charge carriers, ion migration, and ferroelectricity, which are related to grain size and defect density.^{50,51} The **Type C** perovskite with the combination of Lewis base and Lewis acid shows the largest grain size, lowest trap density, highest carrier mobility, and highest conductivity resulting in the most negligible hysteresis. The stabilized power outputs from devices based on pristine, Type A, Type B, and Type C perovskite films are 19.1%, 20.3%, 20.4%, and 21.5%, respectively (**Figure 5e**), which are consistent with the obtained PCEs.

The incident photon-to-electron conversion efficiency (IPCE) spectra of the cells based on the corresponding perovskite layers are presented in **Figure 5f**. The integrated current densities estimated from the IPCE spectra are: 21.6, 22.1, 22.2, and 22.7 mA cm⁻² for pristine, **Type A**, **Type B**, and **Type C** perovskite film-based solar cells, respectively. These results are in good agreement with the *J*_{sc} values obtained from the *J*-*V* curves. The reproducibility of the device performance was evaluated by characterizing

about 20 cells. Histograms of the PCE parameters of these devices (**Figures 6a-d**) indicate excellent reproducibility.

The long-term stability of PSCs is a challenging issue and can be significantly impacted by choice of device architecture that will modulate the role of atmosphere.⁵² The initial stability data of PSC is shown in **Figure 6e,f** and **S8** for tests of the corresponding PSCs without encapsulation under an ambient environment of 10%–20% relative humidity at 20–25 °C and under continuous full-sun illumination at the maximum power-point tracking in a nitrogen atmosphere at 55°C. These studies provide clear evidence that the use of bis-PCBM and BrPh-ThR do not introduce any additional instability for the active layers in this device architecture, and the device based on the combination of BrPh-ThR and bis-PCBM presents a further, very substantial increase in stability over the control device. For example, **Figure 6e** shows the **Type C** device using the combination of BrPh-ThR and bis-PCBM maintained 93.2% of its initial PCE after 3,600 h without encapsulation; under the same conditions, the measured PCEs decreased to 71.7%, 67.6%, and 32.6% of their initial values, respectively, in the **Type B**, **Type A**, and pristine perovskite-based devices. Stability data presented in **Figure 6f** indicate that there is only a 10% efficiency drop after 1,500 h of continuous 1-sun illumination in a nitrogen atmosphere with maximum power-point tracking for a **Type C** PSC. At the same time, the PCEs decreased by 23.6%, 32.1% and 86.1% of their initial values, respectively, in the **Type B**, **Type A**, and pristine perovskite-based solar cells. The **Type C** perovskite solar cells also presented a better stability than that of **Type B**, **Type A**, and pristine perovskite-based solar cells at 85°C in the dark in ambient environment of 10%–20% relative humidity without any encapsulation as shown in **Figure S9**. The improved efficiency without compromise in stability for these device architectures indicates the use of both Lewis base BrPh-ThR and Lewis acid bis-PCBM in perovskite preparation can further enhance PSC stability and technological viability. This is consistent with the ability of this treatment to limit defects-enhanced interaction between organic species (MA and FA), impacting the [PbX₆]⁴⁻ (X: Br and I) octahedral as well as limiting the other moisture-sensitive defects (Pb²⁺). The structural, morphological, and hydrophobicity that result in defect passivation also appear to result in practical improvements that aid stability (e.g., fewer pinholes in the spiro-OMeTAD layer (**Figure S10**), larger grain size, less pronounced boundaries), which should translate into improvements in other device architectures.^{22,49,50,53,54}

Conclusions

In conclusion, we have demonstrated PSCs with simultaneously improved device performance and stability by combining Lewis base BrPh-ThR in the perovskite-solution precursor and Lewis acid bis-PCBM in the antisolvent during the device fabrication for the first time. The Lewis base BrPh-ThR and Lewis acid bis-PCBM can enhance resistance to moisture incursion, passivate the defects in the absorber layer, and suppress pinholes generated in the hole-transporting layer. The combination of Lewis base BrPh-ThR and Lewis acid bis-PCBM positively enhances the crystallization, mobility, and conductivity of perovskites. These beneficial factors lead to much improved device performance and stability. This promising approach provides a simple route for fabricating highly efficient and stable bulk-heterojunction PSCs.

Acknowledgements

We thank Mr. Linfeng Pan from LSPM for Hall Effect tests, Mr. Hongwei Zhu from Tianjin University for ^1H NMR and SCLC tests, and Dr. Rothenberger Guido from LPI for the TRPL analysis. M.G. and S.M.Z. are grateful to the Swiss National Science Foundation for the joint project IZLRZ2_164061 under the Scientific & Technological Cooperation Program Switzerland-Russia, the European Union's Horizon 2020 research and innovation program (under grant agreement No 687008, GOTSolar) and the King Abdulaziz City for Science and Technology (KACST) for financial support. F.Z., K.Z., Z.L. and J.J.B. were supported by the U.S. Department of Energy under Contract No. DE-AC36-08GO28308 with Alliance for Sustainable Energy, LLC, the manager and operator of the National Renewable Energy Laboratory. The authors acknowledge support from the hybrid perovskite solar cell program of the National Center for Photovoltaics, funded by the U.S. Department of Energy, Office of Energy Efficiency and Renewable Energy, Solar Energy Technologies Office. The views expressed in the article do not necessarily represent the views of the DOE or the U.S. Government. The U.S. Government retains and the publisher, by accepting the article for publication, acknowledges that the U.S. Government retains a nonexclusive, paid-up, irrevocable, worldwide license to publish or reproduce the published form of this work, or allow others to do so, for U.S. Government purposes.

Notes and references

§ Competing interests: The authors declare no competing interests.

§ Author contributions: F.Z. designed the experiment, carried out the experimental study on device fabrication, and performed

basic characterization. F.Z. and D.Q.B. performed the PL and contact-angles test. N.M., D.Q.B., and F.Z. performed the stability test. C.X.X. performed the AFM test. Z.L. and F.Z. performed SEM and XRD measurements. F.Z. wrote the first draft of the paper. All authors made a substantial contribution to the discussion of the content and reviewed and edited the manuscript before submission. S.M.Z. coordinated the research, and K.Z. and M.G. supervised the project.

- 1 M. Saliba, T. Matsui, K. Domanski, J.-Y. Seo, A. Ummadisingu, S. M. Zakeeruddin, J.-P. Correa-Baena, W. R. Tress, A. Abate, A. Hagfeldt and M. Gratzel, *Science*, 2016, **354**, 206–209.
- 2 NREL. Best Research-Cell Efficiencies, http://www.nrel.gov/ncpv/images/efficiency_chart.jpg. (May 2018)
- 3 S. S. Shin, E. J. Yeom, W. S. Yang, S. Hur, M. G. Kim, J. Im, J. Seo, J. H. Noh and S. I. Seok, *Science*, 2017, **356**, 167–171.
- 4 W. S. Yang, J. H. Noh, N. J. Jeon, Y. C. Kim, S. Ryu, J. Seo and S. I. Seok, *Science*, 2015, **348**, 1234–1237.
- 5 D. Bi, C. Yi, J. Luo, J.-D. Decoppet, F. Zhang, S. M. Zakeeruddin, X. Li, A. Hagfeldt and M. Gratzel, *Nat. Energy*, 2016, **1**, 16142.
- 6 Q. Chen, H. Zhou, Z. Hong, S. Luo, H. S. Duan, H. H. Wang, Y. Liu, G. Li and Y. Yang, *J. Am. Chem. Soc.*, 2014, **136**, 622–625.
- 7 X. Li, D. Bi, C. Yi, J.-D. Decoppet, J. Luo, S. M. Zakeeruddin, A. Hagfeldt and M. Gratzel, *Science*, 2016, **353**, 58–62.
- 8 Z. Xiao, Y. Yuan, Y. Shao, Q. Wang, Q. Dong, C. Bi, P. Sharma, A. Gruverman and J. Huang, *Nat. Mater.*, 2014, **14**, 193–198.
- 9 M. Liu, M. B. Johnston and H. J. Snaith, *Nature*, 2013, **501**, 395–398.
- 10 M. Xiao, F. Huang, W. Huang, Y. Dkhissi, Y. Zhu, J. Etheridge, A. Gray-Weale, U. Bach, Y.-B. Cheng and L. Spiccia, *Angew. Chem., Int. Ed.*, 2014, **126**, 10056.
- 11 G. Xing, N. Mathews, S. S. Lim, N. Yantara, X. Liu, D. Sabba, M. Gratzel, S. Mhaisalkar and T. C. Sum, *Nat. Mater.*, 2014, **13**, 476–480.
- 12 J. A. Christians, P. Schulz, J. S. Tinkham, T. H. Schloemer, S. P. Harvey, B. J. T. de Villiers, A. Sellinger, J. J. Berry and J. M. Luther, *Nat. Energy*, 2018, **3**, 68–74.
- 13 T. A. Berhe, W.-N. Su, C.-H. Chen, C.-J. Pan, J.-H. Cheng, H.-M. Chen, M.-C. Tsai, L.-Y. Chen, A. A. Dubale and B.-J. Hwang, *Energy Environ. Sci.*, 2016, **9**, 323–356.
- 14 N. H. Tiep, Z. L. Ku and H. J. Fan, *Adv. Energy Mater.*, 2016, **6**, 1501420.
- 15 N. K. Noel, A. Abate, S. D. Stranks, E. S. Parrott, V. M. Burlakov, A. Goriely and H. J. Snaith, *ACS Nano*, 2014, **8**, 9815–9821.
- 16 Y. Lin, L. Shen, J. Dai, Y. Deng, Y. Wu, Y. Bai, X. Zheng, J. Wang, Y. Fang, H. Wei, W. Ma, X. C. Zeng, X. Zhan and J. Huang, *Adv. Mater.*, 2017, **29**, 1604545.
- 17 C. Fei, B. Li, R. Zhang, H. Fu, J. Tian and G. Cao, *Adv. Energy Mater.*, 2017, **7**, 1602017.
- 18 J.-W. Lee, H.-S. Kim and N.-G. Park, *Acc. Chem. Res.*, 2016, **49**, 311–319.
- 19 L. Zhu, Y. Xu, P. Zhang, J. Shi, Y. Zhao, H. Zhang, J. Wu, Y. Luo, D. Li and Q. Meng, *J. Mater. Chem. A*, 2017, **5**, 20874–20881.
- 20 H. Zhu, F. Zhang, Y. Xiao, S. Wang and X. Li, *J. Mater. Chem. A*, 2018, **6**, 4971–4980.
- 21 T. Niu, J. Lu, R. Munir, J. Li, D. Barrit, X. Zhang, H. Hu, Z. Yang, A. Amassian, K. Zhao and S. F. Liu, *Adv. Mater.* 2018, **30**, 1706576.
- 22 G. Yang, P. L. Qin, G. J. Fang, G. Li, *Sol. RRL*, 2018, 1800055.
- 23 M. Sun, F. Zhang, H. Liu, X. Li, Y. Xiao and S. Wang, *J. Mater. Chem. A*, 2017, **5**, 13448–13456.
- 24 K. Liu, S. Dai, F. Meng, J. Shi, Y. Li, J. Wu, Q. Meng and X. Zhan, *J. Mater. Chem. A*, 2017, **5**, 21414–21421.
- 25 M. Qin, J. Cao, T. Zhang, J. Mai, T.-K. Lau, S. Zhou, Y. Zhou, J. Wang, Y.-J. Hsu, N. Zhao, J. Xu, X. Zhan and X. Lu, *Adv. Energy Mater.*, 2018, **8**, 1703399.

- 26 F. Meng, K. Liu, S. Dai, J. Shi, H. Zhang, X. Xu, D. Li and X. Zhan, *Mater. Chem. Front.*, 2017, **1**, 1079–1086.
- 27 M. Zhang, J. Wang, L. Li, G. Zheng, K. Liu, M. Qin, H. Zhou and X. Zhan, *Adv. Sci.*, 2017, **4**, 1700025
- 28 F. Zhang, W. D. Shi, J. S. Luo, N. Pellet, C. Y. Yi, X. Li, X. M. Zhao, T. J. S. Dennis, X. G. Li, S. R. Wang, Y. Xiao, S. M. Zakeeruddin, D. Q. Bi and M. Grätzel, *Adv. Mater.*, 2017, **29**, 1606806.
- 29 K. Wang, C. Liu, P. C. Du, J. Zheng, X. Gong, *Energy Environ. Sci.*, 2015, **8**, 1245–1255.
- 30 C. H. Chiang, C. G. Wu, *Nat. Photonics*, 2016, **10**, 196–200.
- 31 M. Abdi-Jalebi, Z. Andaji-Garmaroudi, S. Cacovich, C. Stavarakas, B. Philippe, J. M. Richter, M. Alsari, E. P. Booker, E. M. Hutter, A. J. Pearson, S. Lilliu, T. J. Savenije, H. Rensmo, G. Divitini, C. Ducati, R. H. Friend and S. D. Stranks, *Nature*, 2018, **555**, 497–501.
- 32 Z. Tang, T. Bessho, F. Awai, T. Kinoshita, M. M. Maitani, R. Jono, T. N. Murakami, H. Wang, T. Kubo, S. Uchida and H. Segawa, *Sci. Rep.*, 2017, **7**, 12183.
- 33 J. Jin, H. Li, C. Chen, B. Zhang, L. Xu, B. Dong, H. Song and Q. Dai, *ACS Appl. Mater. Interfaces*, 2017, **9**, 42875–42882.
- 34 K. Domanski, E. A. Alharbi, A. Hagfeldt, M. Grätzel, W. Tress, *Nat. Energy*, 2018, **3**, 61–67.
- 35 E. M. Sanehira, B. J. Tremolet de Villers, P. Schulz, M. O. Reese, S. Ferrere, K. Zhu, L. Y. Lin, J. J. Berry and J. M. Luther, *ACS Energy Lett.*, 2016, **1**, 38–45.
- 36 X. Zheng, B. Chen, J. Dai, Y. Fang, Y. Bai, Y. Lin, H. Wei, X. C. Zeng and J. Huang, *Nat. Energy*, 2017, **2**, 17102.
- 37 J. Xu, A. Buin, A. H. Ip, W. Li, O. Voznyy, R. Comin, M. Yuan, S. Jeon, Z. Ning, J. J. McDowell, P. Kanjanaboos, J.-P. Sun, X. Lan, L. N. Quan, D. H. Kim, I. G. Hill, P. Maksymovych and E. H. Sargent, *Nat. Commun.*, 2015, **6**, 7081.
- 38 A. Abate, M. Saliba, D. J. Hollman, S. D. Stranks, K. Wojciechowski, R. Avolio, G. Grancini, A. Petrozza and H. J. Snaith, *Nano Lett.*, 2014, **14**, 3247–3254.
- 39 Q. Dong, Y. Fang, Y. Shao, P. Mulligan, J. Qiu and J. Huang, *Science*, 2015, **347**, 967–970.
- 40 M. M. Tavakoli, D. Q. Bi, L. F. Pan, A. Hagfeldt, S. M. Zakeeruddin, M. Grätzel, *Adv. Energy Mater.*, 2018, 1800275.
- 41 Y. Wu, X. Yang, W. Chen, Y. Yue, M. Cai, F. Xie, E. Bi, A. Islam and L. Han, *Nat. Energy*, 2016, **1**, 16148.
- 42 L. L. Jiang, Z. K. Wang, M. Li, C. C. Zhang, Q. Q. Ye, K. H. Hu, D. Z. Lu, P. F. Fang and L. S. Liao, *Adv. Funct. Mater.*, 2018, **28**, 1705875.
- 43 Z. Liu, J. Hu, H. Jiao, L. Li, G. Zheng, Y. Chen, Y. Huang, Q. Zhang, C. Shen, Q. Chen and H. Zhou, *Adv. Mater.*, 2017, **29**, 1606774.
- 44 X. Zhang, X. Ren, B. Liu, R. Munir, X. Zhu, D. Yang, J. Li, Y. Liu, D.-M. Smilgies, R. Li, Z. Yang, T. Niu, X. Wang, A. Amassian, K. Zhao and S. Liu, *Energy Environ. Sci.*, 2017, **10**, 2095–2102.
- 45 J.-W. Lee, S.-H. Bae, Y.-T. Hsieh, N. De Marco, M. Wang, P. Sun and Y. Yang, *Chem*, 2017, **3**, 290–302.
- 46 D.-Y. Son, J.-W. Lee, Y. J. Choi, I.-H. Jang, S. Lee, P. J. Yoo, H. Shin, N. Ahn, M. Choi and D. Kim, *Nat. Energy*, 2016, **1**, 16081.
- 47 Z. K. Wang, X. Gong, M. Li, Y. Hu, J. M. Wang, H. Ma and L. S. Liao, *ACS Nano*, 2016, **10**, 5479.
- 48 C. Li, J. Sleppy, N. Dhasmana, M. Soliman, L. Tetard, J. Thomas, *J. Mater. Chem. A*, 2016, **4**, 11648–11655 (2016).
- 49 D. Bi, W. Tress, M. I. Dar, P. Gao, J. Luo, C. Renevier, K. Schenk, A. Abate, F. Giordano, J. P. Correa Baena, J. D. Decoppet, S. M. Zakeeruddin, M. K. Nazeeruddin, M. Grätzel and A. Hagfeldt, *Sci. Adv.*, 2016, **2**, e1501170
- 50 Z. Chu, M. Yang, P. Schulz, D. Wu, X. Ma, E. Seifert, L. Sun, X. Li, K. Zhu and K. Lai, *Nat. Commun.*, 2017, **8**, 2230.
- 51 Y. Yuan, J. S. Huang, *Acc. Chem. Res.*, 2016, **49**, 286–293.
- 52 X. Li, M. I. Dar, C. Y. Yi, J. S. Luo, M. Tschumi, S. M. Zakeeruddin, M. K. Nazeeruddin, H. W. Han and M. Grätzel, *Nat. Chem.*, 2015, **7**, 703–711.
- 53 H. Back, G. Kim, J. Kim, J. Kong, T. K. Kim, H. Kang, H. Kim, J. Lee, S. Lee and K. Lee, *Energy Environ. Sci.*, 2016, **9**, 1258–1263.
- 54 F. Zhang, C. Y. Yi, P. Wei, X. D. Bi, J. S. Luo, G. Jacopin, S. R. Wang, X. G. Li, Y. Xiao, S. M. Zakeeruddin and M. Grätzel, *Adv. Energy Mater.*, 2016, **6**, 1600401.

Synergistic combination of Lewis base and Lewis acid enables perovskite solar cell with high efficiency and stability.

